IEEE Photonics Journal
An IEEE Photonics Society Publication

Open Access

Development of an Aspherical Aerial Camera Optical System

Volume 11, Number 6, December 2019

Jieqiong Lin
Chenping Jiang
Mingming Lu
Minghui Gao
Qing Guo

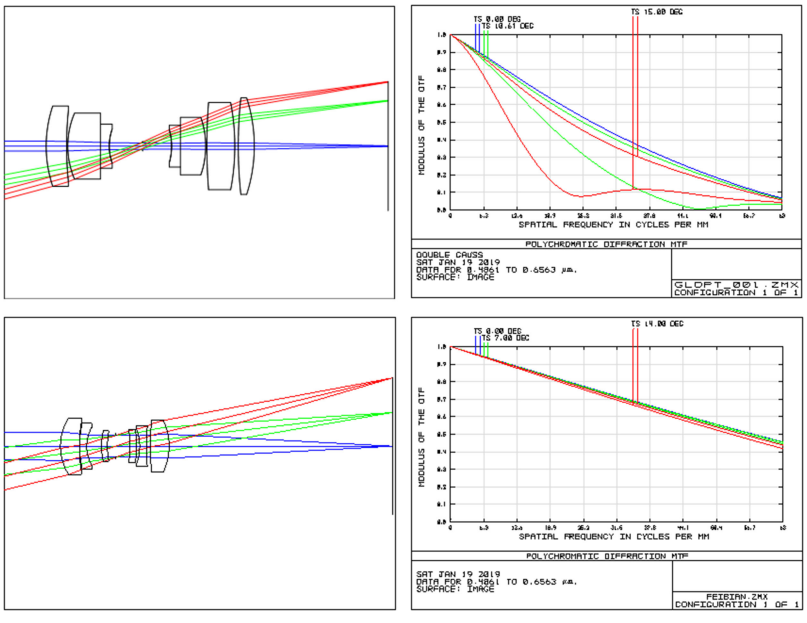

DOI: 10.1109/JPHOT.2019.2950038

Development of an Aspherical Aerial Camera Optical System

Jieqiong Lin,[1] **Chenping Jiang**,[1] **Mingming Lu**,[1] **Minghui Gao**,[2] **and Qing Guo**[1]

[1]Key Laboratory of Micro/Nano and Ultra-precision Manufacturing (Jilin Province), School of Mechatronic Engineering, Changchun University of Technology, Changchun 130012, China
[2]Fine Mechanics and Physic, Chinese Academy of Sciences, Changchun Institute of Optics, Changchun 3888, China

DOI:10.1109/JPHOT.2019.2950038

Manuscript received August 20, 2019; revised October 7, 2019; accepted October 24, 2019. Date of publication October 28, 2019; date of current version December 16, 2019. This paper was supported in part by the Ministry of Science and Technology State Key Support Program under Grant 2016YFE0105100, in part by the Micro-Nano and Ultra-Precision Key Laboratory of Jilin Province under Grant 20140622008JC, and in part by the Education Department Scientific Research Planning Project of Jilin Provincial under Grant JJKH20181038KJ and 20180101034JC. Corresponding author: Mingming Lu (e-mail: lumm@ccut.edu.cn).

Abstract: The aerial camera lens largely determines the performance of the camera. It is necessary to further optimize the lens to satisfy the requirements of small-scale and lightweight aircraft camera systems. The optical system design is the primary prerequisite. Therefore, considering the image quality and working environment of the aerial camera, an aspherical aerial camera optical system is developed by studying the aerial camera optical system. The work presented in this paper decreases the overall weight of the aerial camera by using an aspherical lens instead of a spherical lens, which reduces the number of lenses and improves the image quality. The athermalization of the optical system ensures that the camera has good temperature adaptability in the temperature range of -60 °C$\sim$60 °C. The definition of the aspherical surface shape is detected by a ZYGO digital interferometer. The root mean square (RMS) of the system is $0.0403\lambda(\lambda = 632$ nm), and the peak value (PV) is 0.354λ, which ensures the image quality of the camera. The research results verify that the aspherical lens can be well applied to the camera optical system, improving the image quality of the system and reducing the weight of the camera.

Index Terms: Aerial camera, optical system, aspherical, image quality.

1. Introduction

Aerial camera is an optical instrument mounted on the plane that captures ground target information by photographing surface scenery. Advances in computer technology, communication technology and network technology have promoted the development of aviation camera technology and the progress of information processing technology. Aviation cameras have experienced a development process from nothing to existence, from poverty to wealth [1]–[5]. With the wide application of aerial camera technology, the performance requirements of aerial camera are increasing.

The performance of aerial cameras is largely determined by the aerial camera optics. Designers have used methods to improve the optical performance and image quality of various optical systems to meet the needs of society [6]–[8]. The aspherical lens has a more suitable curvature. It can maintain good aberration correction to achieve the desired performance [9]. Therefore, the use of aspherical lenses makes the design of optical systems more complex and diverse. Chernomyrdin

N V, Frolov M E, *et al*. made use of wide-aperture aspherical lenses for high-resolution terahertz imaging [10]. Cheng D, Gong C, *et al*. improved the image quality of the system by applying annularly stitched aspherical surface (AAS) to the back surface of the catadioptric element [11]. Qin H, Lei C, Liu H *et al*. designed an aspherical cylindrical reflective solar collector [12]. Wu R, Hua H, *et al*. developed compact and ultra efficient aspherical lenses for extended Lambertian sources in two-dimensional geometry [13]. The application of aspherical lenses brings excellent sharpness and higher resolution. The miniaturization of the lens can also be achieved by aspherical lenses.

With the continuous advancement of aspherical surface processing and inspection technology, the manufacturing cost of aspherical lenses is reduced and the precision is improved. Researches prove that the application of aspherical lenses is increasingly widespread. The development of aspherical manufacturing technology makes aspherical applications in aerial cameras possible. M T Langridge, D C Cox, *et al*. demonstrated a technique for creating bespoke, highly-accurate aspheric or spherical profile silicon microlens moulds, of almost any footprint, using focused ion-beam milling [14]. Cao, Zhaolou, Wang, Keyi, *et al*. proposed a novel method to fabricate aspherical anamorphic lenses at very low costs [15]. W. Liao, Y. Dai, *et al*. proposed a combined technique that includes magnetorheological finishing, smoothing polishing, and IBF [16]. Jiang Zi Bo, Li Xin Nan *et al*. established an elastic model that corrects the spherical aberration by applying a central lateral load [17]. In this paper, an aspherical lens is applied to the optical system of an aerial camera to decrease the number of lenses and thus cut down the overall weight of the aerial camera. The initial structure of the aerial camera optical system is optimized and the image quality is further improved.

The chapters of this paper are distributed as follows: The second part mainly introduces the optimization design of optical system. The operating temperature environment of the camera optics is described in the third section. The fourth part uses the ZYGO digital interferometer to detect the surface accuracy of the aspherical surface and the image quality of the system is detected by the scene generator. Finally, the conclusion is reflected in the fifth part.

2. Optical System Design

2.1 Initial Structure Design of Optical System

Typical structures for optical systems include reflective system, refractive system, and catadioptric system. The reflective system is mainly suitable for large F-number and small field of view applications. This type of system effectively compresses the optical path length, making the system size much smaller than the system focal length. The disadvantages are that few available variables, insufficient ability of off-axis aberration correction, and small realizable field of view. The refracted system is a coaxial system that can achieve a large field-of-view angle. After the general system enlarges the angle of view, astigmatism and curvature of field and distortion become difficult to correct. When the relative aperture is increased, various advanced spherical aberrations become the main factors affecting the image quality. The advantage of the catadioptric system is that the system power is concentrated almost entirely on the reflecting surface, and the reflecting surface does not produce chromatic aberration. The catadioptric system has the characteristics of simple structure, short length and light weight. However, the shortcoming of the catadioptric system is that the energy loss and the reduction in the modulation transfer function (MTF) result from the obstruction in the central part of the system. Considering the difficulty of optical design and the surface obscuration in the optical system, it was finally decided to use the refractive optical system.

In this paper, a refractive optical system with focal length $f'' = 80$ mm, aperture $\Phi = 10$ mm, field of view $W = 28°$, working spectrum of 380$\sim$780 nm is designed. The size of the image sensitive unit of the charge coupled diode (CCD) (VT-3/4/6 KC, VIEWORKS, Korea) image sensor is 8 um, and the Nyquist frequency of the system is obtained as $f_N = 1/2a = 62.5$ p/mm, and optical evaluation is performed at 63 lp/mm.

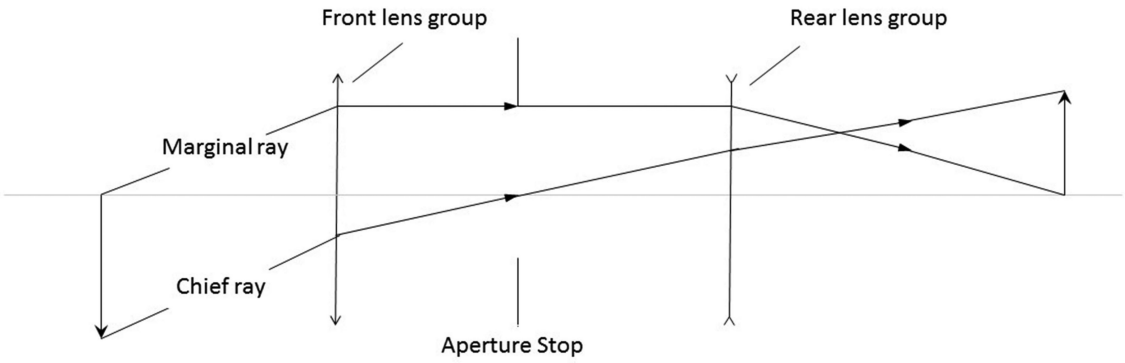

Fig. 1. Schematic diagram of optical system structure.

The schematic diagram of the optical system structure can be seen from Figure 1. The whole system is divided into two lens groups. The aperture is placed in the middle of the two lens groups to correct the out-of-axis aberration. The focal length is scaled according to the structure of the optical system. The scaling of focal length is shown in Formula 1.

$$K = \frac{f''}{f'}, \tag{1}$$

where K is a scaling factor, f' is the focal length of existing structure, f'' is the focal length to be designed. The scaled structural parameters are shown in Formula 2.

$$\begin{cases} r'' = r'K = r'\frac{f''}{f'} \\ d'' = d'K = d'\frac{f''}{f'} \end{cases}, \tag{2}$$

where r' is the radius of curvature of the existing structure, r'' is the radius of curvature of the scaled structure, d' is the lens thickness or spacing of the existing structure, d'' is the lens thickness or spacing of the scaled structure. Change the glass material after determining the radius and spacing of curvature. The glass closes to the dispersion coefficient is selected to keep the color difference constant or small and the curvature radius of the glass-replaced lens is modified accordingly to ensure that the focal degree of the lens does not change. The boundary conditions are finally defined and aberration correction is performed.

We can see from as schematized in Figure 2, that the optical system optical path obtained by using the optical design software ZEMAX is optimized according to the requirements of the optical system design.

The optical system is now a full refraction system with seven spherical lenses. Figure 3 shows the MTF of the Spherical system. It can be seen that the MTF value cannot meet the technical requirements within the maximum spatial frequency of 63 lp/mm. The S curve (sagittal curve) and the T curve (meridian curve) have a large deviation and a large astigmatism.

The distortion of the system can be seen from the Figure 4. The distortion curve takes the image height Y as the vertical coordinate and the distortion as the transverse coordinate. The distortion at the edge field of view is within 2.5%, and the distortion becomes a good correction.

Figure 5 shows the spot diagram of the system. From the Figure 5, we can see that the airy radius of the system is 16.7 μm in diameter, and the maximum diameter of the diffuse spot is 40.723 μm, which is larger than the diameter of the airy radius and does not meet the imaging requirements.

2.2 Optical System Optimization

The spherical lens has only a constant curvature from the center to the edge, and there is only one freedom designed in the design process. The curvature of the aspherical lens changes continuously

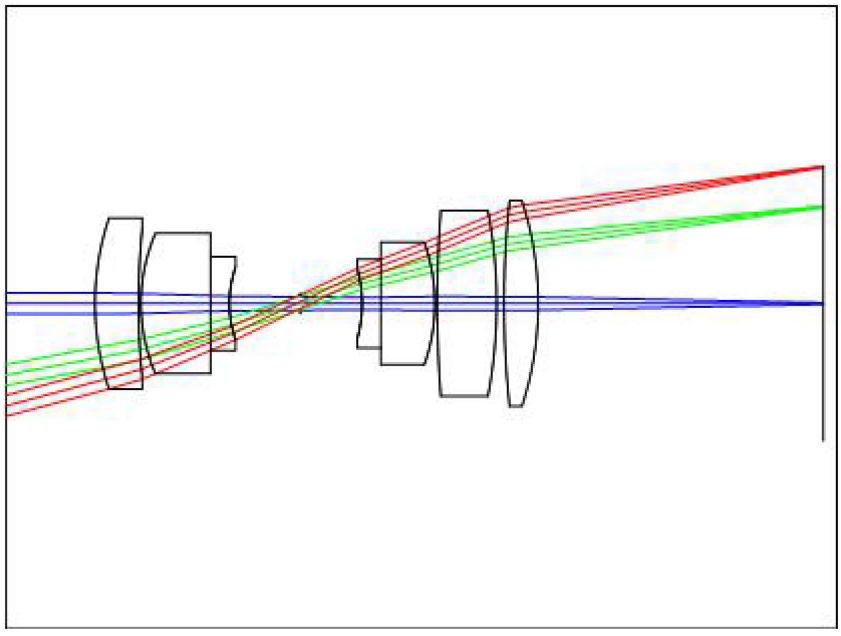

Fig. 2. Spherical structure of the initial structure.

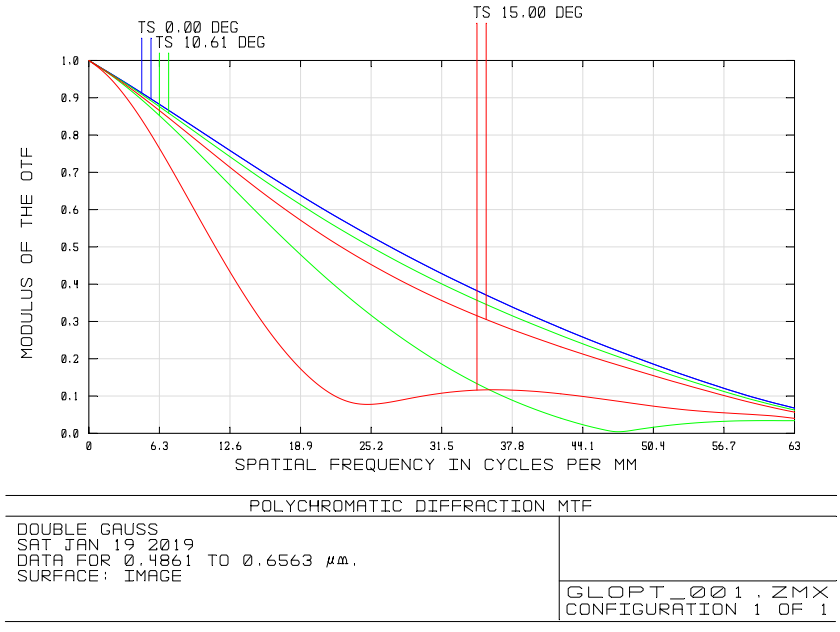

Fig. 3. Spherical system MTF evaluation results.

from the center to the edge. Theoretically, there are infinite degrees of freedom in design. Therefore, it has a huge advantage in terms of aberrations compared to a spherical lens. Introducing aspherical surface into the system design can improve the optical performance and image quality of the lens, decrease the number of lenses, and simplify the lens structure. Set the fourth surface in the initial structure to aspherical and delete the sixth spherical lens. The optical system after continuous optimization can be seen from Figure 6.

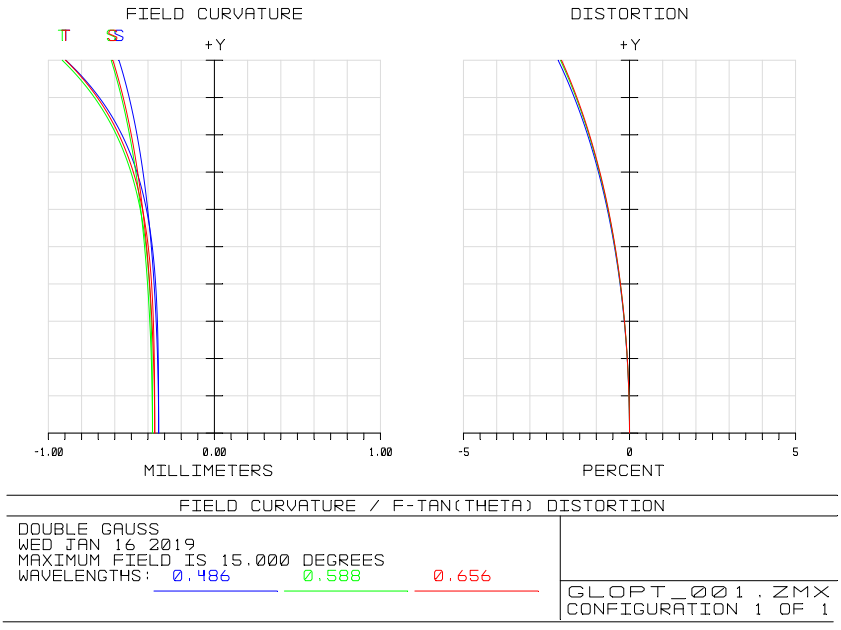

Fig. 4. Spherical system distortion diagram.

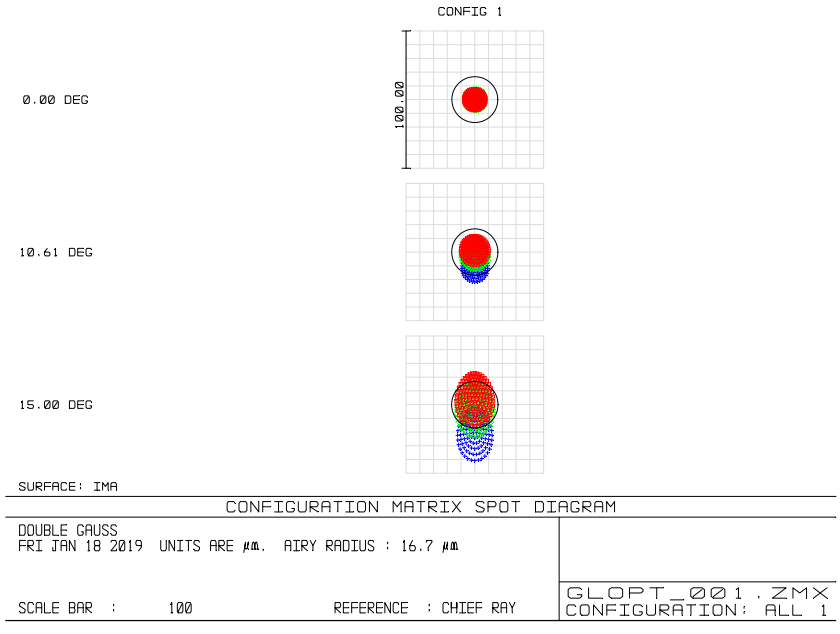

Fig. 5. Spherical system spot diagram.

The structural parameters of the optimized system with aspherical surface are shown in Table 1. The table contains the type of lens, radius of curvature, thickness, material, and through-light aperture of the system. As can be seen from the table, the fourth surface is an aspherical lens.

The aspherical is the fourth surface and the parameter is shown in Table 2. The coefficients of its high-order aspherical surface are listed in the table.

As Figure 7 obviously shows, the transfer functions of all fields of view are close to the diffraction limit. At 63 lp/mm, the field of view MTF reached 0.4, which is close to the diffraction limit. The

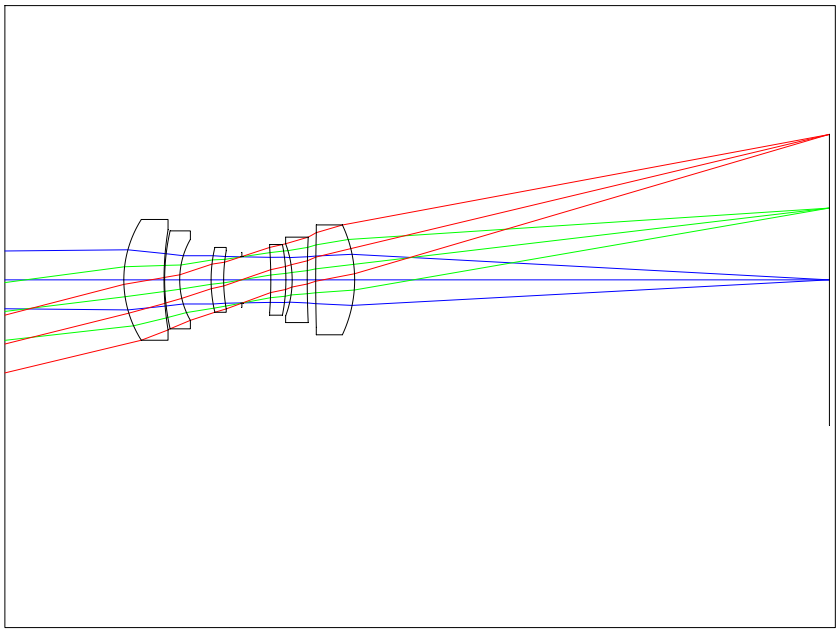

Fig. 6. Optimization system with aspherical surface.

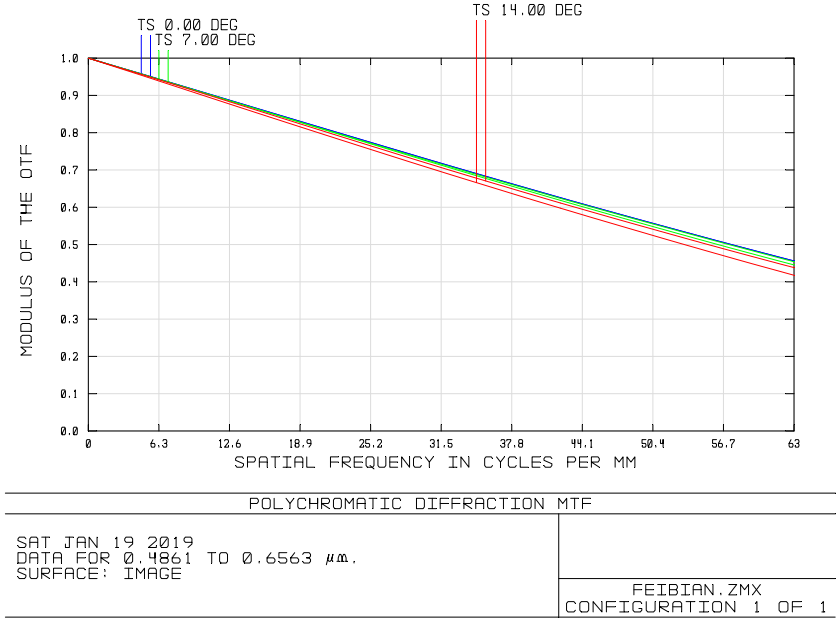

Fig. 7. MTF evaluation results of aspherical systems.

S curve (sagittal curve) coincides with the T curve (meridian curve). The smaller the deviation between the two, the smaller the astigmatism of the lens.

Figure 8 represents the distortion of the system. Distortion is the aberration in which the magnification varies with the field of view. The distortion at the edge field of view is controlled within 0.4% to meet the design requirements.

As can be seen from Figure 9 that the airy radius of the system has a diameter of 7.869 μm. The maximum diameter of the diffuse spot in each field of view is 6.575 μm. Both are smaller than

TABLE 1
Structural System Parameters With Aspherical Surfaces

Surf：	Type	Radius (mm)	Thickness (mm)	Glass	Semi-Diameter (mm)
OBJ	Standard	-	Infinity		
1	Standard	18.046	6.400	HZBAF50	9.631
2	Standard	50.120	0.100		7.993
3	Standard	35.480	2.400	HF13	7.811
4	Even Asphere	13.317	5.000		6.460
5	Standard	24.770	2.000	HZK6	5.171
6	Standard	28.444	2.600		4.639
STO	Standard	1e+018	5.000		3.724
8	Standard	-64.993	2.400	HZK20	5.173
9	Standard	-27.430	0.970		5.633
10	Standard	-16.218	2.400	F2	5.759
11	Standard	192.310	1.320		6.813
12	Standard	402.500	6.200	HZBAF50	7.538
13	Standard	-20.700	62.126		8.764
IMA	Standard	-	0		23.215

the airy disk diameter and less than one cell size. The airy disk surrounds all the points and the image quality of the optical system was significantly improved.

After using aspherical optimization, the aberrations of the system have been greatly improved. The design results show that the distortion of the full field of view is less than 0.4%. The distortion is greatly reduced compared to the spherical system. The deformation of the image is fully improved. The diameter of the airy radius decreased from 16.7 μm to 7.869 μm. The maximum diameter of the diffuse spot decreased from 40.723 μm to 6.575 μm. The resolution of the image surface of the optical system is increased. The MTF values are increased to above 0.4. Compared to the spherical system, the MTF curve is more straight and the edge is more consistent with the middle. By using an aspherical lens, the edge contrast and resolution of the image are improved. The number of lenses has been decreased from 7 to 6 to reduce system weight.

3. Athermalization

Under normal circumstances, an optical system is designed, which is used at normal temperature and pressure. However, for the aeronautical optical system, the environmental conditions of

TABLE 2
Aspherical Parameters

Aspherical high order	coefficient
Quadric surface	0.144
Sixth order aspherical	-3.04E-09
Eighth order aspherical	1.62E-10

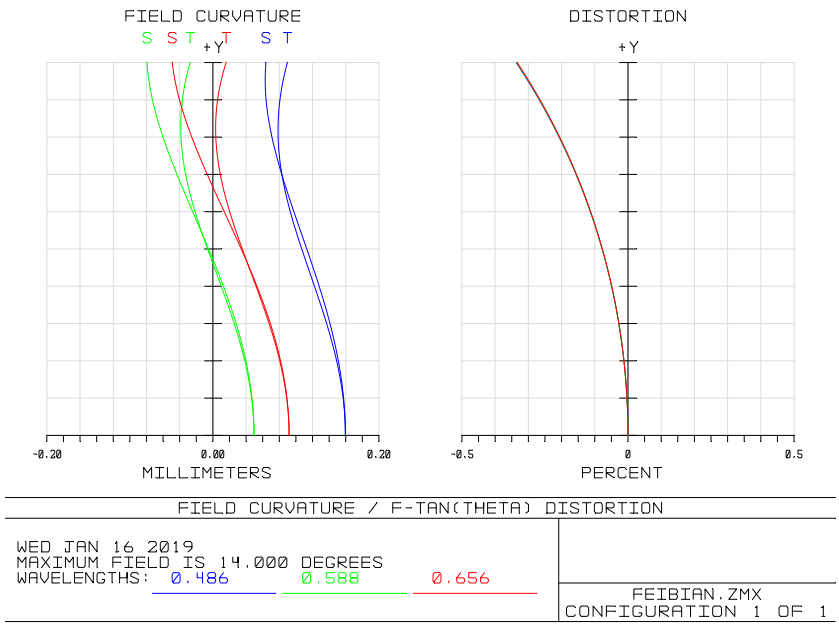

Fig. 8. Field curvature and distortion of an aspherical system.

the optical system are greatly different from the ground with the rise of the flying height, especially the influence of the temperature change on the image quality. Temperature changes cause changes in the refractive index of the medium, which can cause variations in the thickness of the optical components in the optical system, the air separation between the components, and the refraction and reflection surface profiles. With the need for high-quality imaging of aerial cameras, the adiabatic aberration technology of airborne optical systems has also grown considerably.

Optimizing the optical system in different temperature environments can make the system insensitive to temperature changes. The basic idea is to design the optical system at normal temperature first. Optical systems in different temperature environments are then considered as different optical structures in optical design software. According to the temperature environment in which the optical system is located. Correlate the expansion coefficient, size, refractive index of the optical material, and the expansion coefficient and size of the structural member. Optimize the optical system in these three temperature environments to achieve athermalization. The optical parameter at a normal temperature of 20 °C is used as a reference for optimization.

The optical system is converted into a triple structure corresponding to the optical parameters of −60 °C, 20 °C and 60 °C. The sellmeier formula used to calculate the change rate of refractive

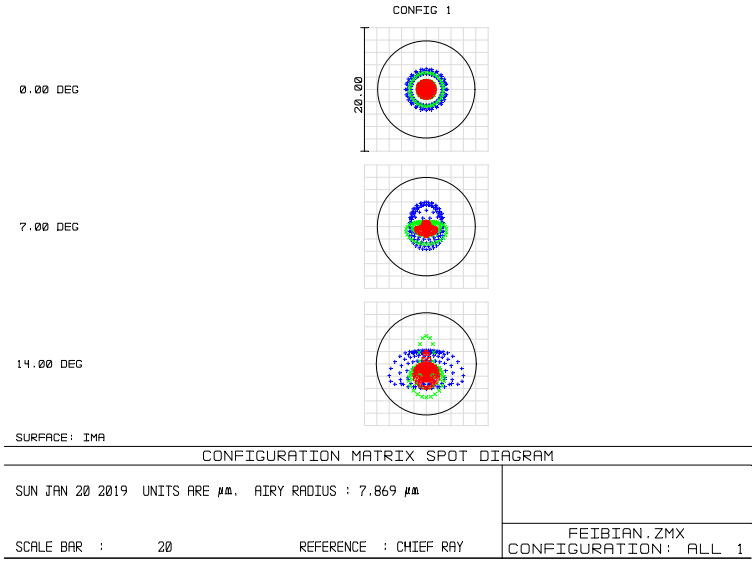

Fig. 9. Spot diagram with aspherical system.

index of optical glass in vacuum is shown in formula 3.

$$\frac{dn_{abs}}{dT} = \frac{n_{rel}^2(\lambda, T_0) - 1}{2n_{rel}(\lambda, T_0)} \left(D_0 + 2D_1\Delta T + 3D_2\Delta T^2 + \frac{E_0 + 2E_1\Delta T}{\lambda^2 - \lambda_{TK}^2} \right), \tag{3}$$

where n_{abs} (at an air pressure of $0.1033{\cdot}10^6$Pa) and n_{rel}(in vacuum) is the refractive index of the glass. T_0 is a temperature standard (usually 20 °C). D_i, E_i and λ_{TK} is a specific coefficient of glass and $\Delta T = T - T_0$. Optimize the triple structure and adapt some of the optical materials as appropriate. After athermalization, the MTF curves of the optical system at −60 °C, 20 °C and 60 °C can be seen from Figure 10(a)–(c).

As schematized in Figure 10(a)–(c), the MTF of the optical system is maintained at 0.4 or higher at −60 °C to 60 °C. The change is very small compared to the optical system MTF at normal temperature. The athermalization design ensures that the camera has good temperature adaptability over a wide temperature range, which is conducive to miniaturization and lightweight design of the aerial camera.

4. Detection and Experiment

4.1 ZYGO Digital Interferometer Detection

High-order aspherical lenses are increasingly used in modern aerial camera optical systems to improve overall system performance. The accuracy of the lens surface shape directly affects the image quality of the lens. Therefore, it is very important to accurately measure the lens surface shape and give a correct evaluation. In the evaluation of the surface accuracy, the PV value and the RMS value are among the more common indicators. The PV value corresponds to the difference between the peak and valley values of the lens wavefront. The RMS value is a kind of statistic that can more objectively reflects the degree of changes in the shape of the lens. As an indispensable quantitative detection technology in the manufacturing technology of high-order aspherical optical components, development is relatively slow due to various factors and conditions. The zero compensation method in the interferometry method has always been the main way of aspherical surface shape detection because of its high precision, convenient adjustment and stability.

The work presented in this paper uses ZYGO digital interferometer to detect the surface of high-order aspherical surface. The surface equation of the high-order aspherical surface to be detected

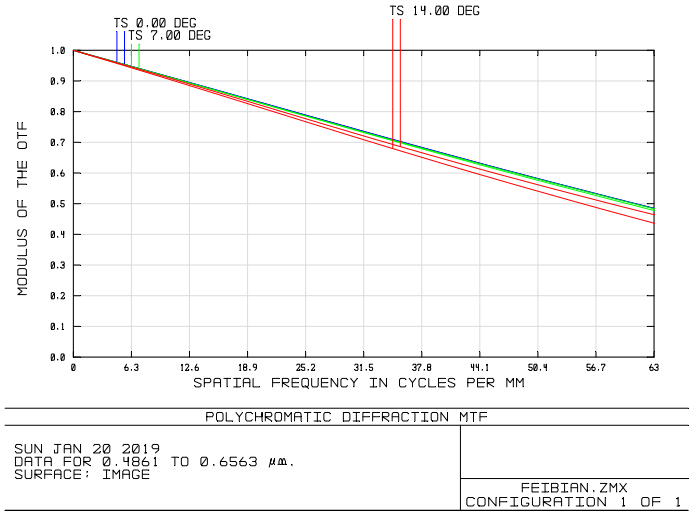

(a)

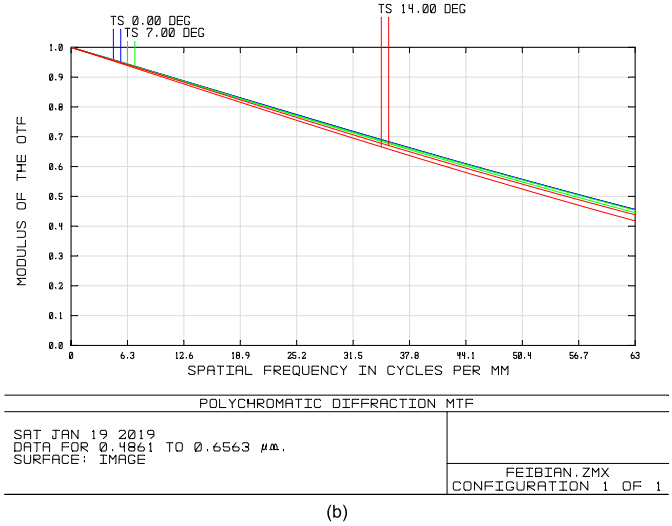

(b)

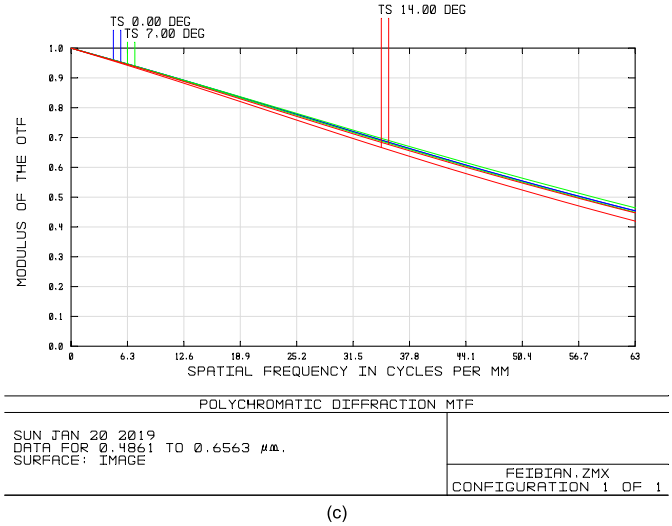

(c)

Fig. 10. When the ambient temperature of the system is (a) −60 °C, (b) 20 °C, and (c) 60 °C, the corresponding MTF value is obtained.

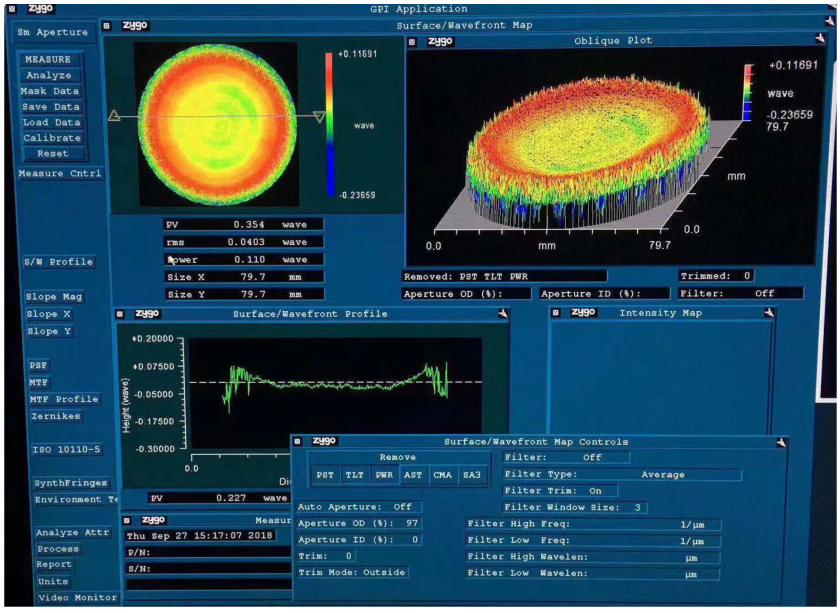

Fig. 11. ZYGO interferometer measurement result chart.

is as shown in Formula (4).

$$z = \frac{cr^2}{1 + \sqrt{1 - (1 + k)c^2 r^2}} + a_4 r^4 + a_6 r^6, \tag{4}$$

where c is the base curvature of the apex, k is the conic constant, $a_i r^i$ is the high order term of the aspherical surface.

The residual wave aberration of the detection system is shown in Figure 11. The RMS value is 0.0403λ ($\lambda = 632$ nm), which is better than 1/20 λ. The PV value is 0.354 λ, and the aspherical surface accuracy is ideal. The measurement results all meet the requirements of the surface error. The change of the lens shape under the working environment is controlled within the specified tolerance range to ensure the image quality of the camera and make the aberrations undisturbed. The test proves that the accuracy of the aspherical lens surface shape is satisfied.

4.2 Optical System Image Quality Testing Experiment

The ground scene generator is used to test the image quality of the camera to verify the image quality of the optical system. The ground scene generator is a device for inspecting and testing aerial cameras in a laboratory environment. Using the ground scene motion seen when the simulated aircraft flies in the air, and based on the combination of similarity principles and information technology. The ground scene generator is evaluated by computer control, optical, automatic control, digital image processing and other technologies to evaluate various indicators and technical requirements of aerial cameras.

The camera image quality measurement site can be seen from Figure 12. The camera was fixed on the mount, and placed the scene generator at the same level as the camera. The distance between the camera and the scene generator was 500 mm. The speed controller was used to set the rotation speed of the scene generator according to the desired speed ratio (The scene generator motion can be set from 10 degrees per second to 200 degrees per second, and the corresponding speed controller setting is 50∼2000). Used the camera for image acquisition in sufficient light conditions.

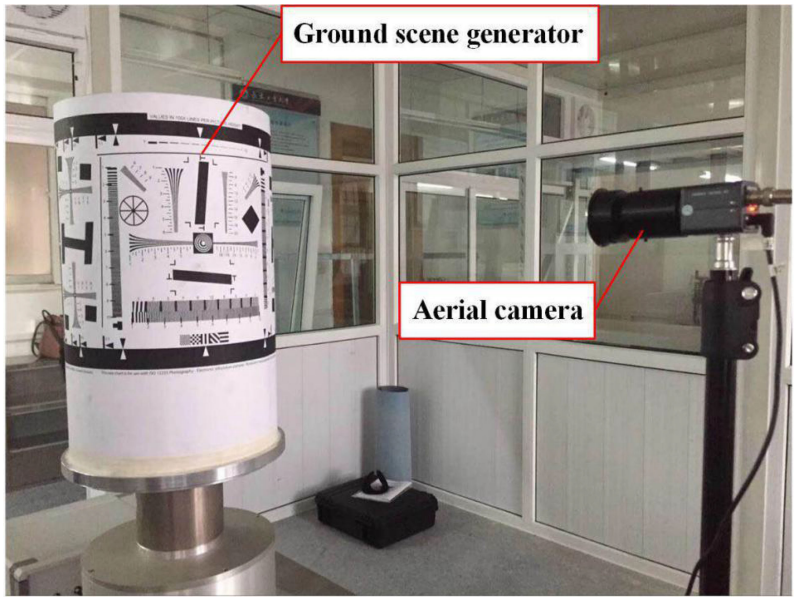

Fig. 12. Ground scene generator.

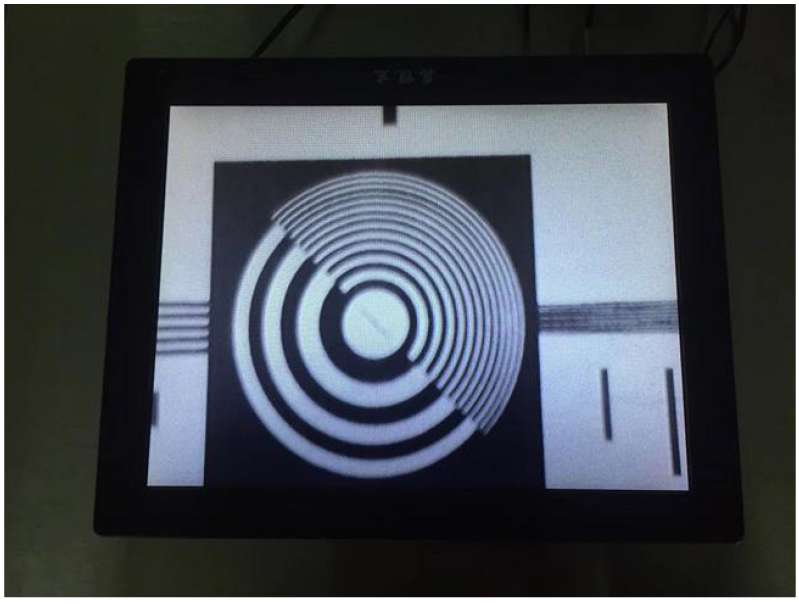

Fig. 13. Image detection result.

Calculate the ground pixel resolution according to formula (5):

$$GSD = \frac{\boldsymbol{b} \times H}{f'' \times \sin\theta}, \tag{5}$$

where b is CCD cell size, b = 0.008 mm; f″ is camera focal length, f″ = 80 mm; H is the vertical distance of the camera from the target, H = 500 mm; θ is camera scan angle, $\theta = 90°$.

The experimental results show that the camera can distinguish the target with a black-and-white spacing of 0.5 mm when the ground scene generator moves at a speed of 150 degrees per second.

As can be seen from Figure 13 that the lines are clearly visible and the image is evenly illuminated without obvious bending, which meets the design requirements.

5. Conclusion

The work presented in this paper develops an optical system of aerial cameras by using aspherical lenses instead of spherical lenses to decrease the number of lenses from seven to six. The overall weight of the aerial camera system is reduced. Through the experimental results, the following conclusions are formed:

1) Optical systems with aspherical surfaces have fewer lenses than spherical optical systems and better image quality than spherical optical systems. The MTF values of each field of view of the optical system containing aspherical surface are greater than 0.4 (@63 lp/mm). The maximum diameter of the diffuse spot is less than 10 μm, and the total field of view distortion is less than 0.4%, which fully meets the system image quality requirements.
2) Non-thermal design, proves that the system has good temperature adaptability in the temperature range of -60 °C$\sim$60 °C. The ZYGO digital interferometer shows that the RMS value of the aspherical is 0.0403 λ and the PV value is 0.354 λ, both satisfy the system design demands. Simultaneously, the camera can distinguish the target with a black-and-white spacing of 0.5 mm clearly. It can be seen that the image quality is outstanding by the experiment.

The design results show that the application of the aspherical lens to the design of the aerial camera optical system can significantly improve the image quality of the camera and reduce the weight of the camera.

References

[1] Z. Szantoi, S. E. Smith, G. Strona, L. P. Koh, and S. A. Wich, "Mapping orangutan habitat and agricultural areas using Landsat OLI imagery augmented with unmanned aircraft system aerial photography," *Int. J. Remote Sens.*, vol. 38, pp. 2231–2245, 2017.

[2] J. Suh and Y. Choi, "Mapping hazardous mining-induced sinkhole subsidence using unmanned aerial vehicle (drone) photogrammetry," *Environ. Earth. Sci.*, vol. 76, no. 4, p. 144, 2017.

[3] M. Bryson *et al.*, "Geomorphic changes of a coral shingle cay measured using Kite Aerial Photography," *Geomorphology*, vol. 270, pp. 1–8, 2017.

[4] E. Rykker and M. Peter, "The application of low-altitude near-infrared aerial photography for detecting clandestine burials using a UAV and low-cost unmodified digital camera," *Forensic Sci. Int.*, vol. 289, pp. 408–418, 2018.

[5] X. X. Li and G. F. Shao, "Object-based urban vegetation mapping with high-resolution aerial photography as a single data source," *Int. J. Remote Sens.*, vol. 34, no. 3, pp. 771–789, 2013.

[6] I. Powell, "Design study of an infrared panoramic optical system," *Appl. Opt.*, vol. 35, no. 31, pp. 6190–6194, 1996.

[7] I. S. Mcdermid, T. Daniel Walsh, A. Deslis, and M. L. White, "Optical systems design for a stratospheric lidar system," *Appl. Opt.*, vol. 34, no. 27, pp. 6201–6210, 1995.

[8] F. B. Patrick and W. H. Scidmore, "Optical system design for telescopes," *Appl. Opt.*, vol. 3, no. 3, pp. 427–431, 1964.

[9] B. Braunecker, H. Rüdiger, and H. J. Tiziani, *Advanced Optics Using Aspherical Elements*. SPIE Press, 2013.

[10] N. V. Chernomyrdin *et al.*, "Wide-aperture aspherical lens for high-resolution terahertz imaging," *Rev. Sci. Instrum.*, vol. 88, no. 1, 2017, Art. no. 014703.

[11] D. Cheng, C. Gong, C. Xu, and Y. Wang, "Design of an ultrawide angle catadioptric lens with an annularly stitched aspherical surface," *Opt. Express*, vol. 24, no. 3, pp. 2664–2677, 2016.

[12] H. Qi, C. Lei, H. Liu, Y. Wang, and W. Yuan, "Optical design of an aspherical cylinder-type reflecting solar concentrator," *Energy*, vol. 57, pp. 751–758, 2013.

[13] R. Wu, H. Hua, P. Benítez, J. C. Miñano, and Rongguang Liang, "Design of compact and ultra efficient aspherical lenses for extended Lambertian sources in two-dimensional geometry," *Opt. Express*, vol. 24, no. 5, pp. 5078–5086, 2016.

[14] M. T. Langridge, D. C. Cox, R. P. Webb, and V. Stolojan, "The fabrication of aspherical microlenses using focused ion-beam techniques," *Micron*, vol. 57, no. 2, pp. 56–66, 2014.

[15] Z. Cao, K. Wang, and Q. Wu, "Aspherical anamorphic lens for shaping laser diode beam," *Opt. Commun.*, vol. 305, pp. 53–56, 2013.

[16] W. Liao, Y. Dai, X. Nie, X. Xie, and C. Song, "Rapid fabrication technique for nanometer-precision aspherical surfaces," *Appl. Opt.*, vol. 54, no. 7, pp. 1629–1638, 2015.

[17] J. Z. Bo *et al.*, "Influence and control of spherical aberration in polishing off-axis aspherical mirrors by the stressed method," *Appl. Opt.*, vol. 54, no. 2, pp. 291–298, 2015.